

The halo mass function in interacting Dark Energy models

Weiguang Cui¹, Marco Baldi^{2,3}, Stefano Borgani^{1,4,5}

¹ *Astronomy Unit, Department of Physics, University of Trieste, via Tiepolo 11, I-34131 Trieste, Italy (wgcai,borgani@oats.inaf.it)*

² *Excellence Cluster Universe, Boltzmannstr. 2, D-85748 Garching, Germany (marco.baldi@universe-cluster.de)*

³ *University Observatory, Ludwig-Maximilians University Munich, Scheinerstr. 1, D-81679 Munich, Germany*

⁴ *INAF, Astronomical Observatory of Trieste, via Tiepolo 11, I-34131 Trieste, Italy*

⁵ *INFN – National Institute for Nuclear Physics, Trieste, Italy*

11 November 2018

ABSTRACT

We present a detailed investigation of the effects that a direct interaction between Dark Energy and Cold Dark Matter particles imprints on the Halo Mass Function of groups and clusters of galaxies. Making use of the public halo catalogs of the CoDECS simulations, we derive the Halo Mass Function for several different types of coupled Dark Energy scenarios both based on the Friends-of-Friends algorithm and on the Spherical Overdensity halo identification for different values of the overdensity threshold Δ_c . We compare the computed Halo Mass Functions for coupled Dark Energy cosmologies with Λ CDM as well as with the predictions of the standard analytic fitting functions. Our results show that the standard fitting functions still reproduce reasonably well both the Friends-of-Friends and the Spherical Overdensity Halo Mass Functions of interacting Dark Energy cosmologies at intermediate masses and at low redshifts, once rescaled to the characteristic amplitude of linear density perturbations of each specific model as given by σ_8 . However, we also find that such apparent degeneracy with σ_8 is broken both by the high-mass tail and by the redshift evolution of our Halo Mass Functions, with deviations beyond $\sim 10\%$ for most of the models under investigation. Furthermore, the discrepancy with respect to the predictions of standard fitting functions rescaled with the characteristic value of σ_8 shows – for some models – a strong dependence on the spherical overdensity threshold Δ_c used for the halo identification. We find that such effect is due to a significant increase of halo concentration at low redshifts in these models, that is however absent in the majority of the cosmological scenarios considered in this work. We can therefore conclude that the universality of the Halo Mass Function is violated by cosmological models that feature a direct interaction between Dark Energy and Cold Dark Matter.

Key words: dark energy – dark matter – cosmology: theory – galaxies: formation

1 INTRODUCTION

Despite its longstanding success in explaining a wide range of astrophysical and cosmological observations, the standard cosmological model based on a cosmological constant Λ as the driver of the observed accelerated expansion (Riess et al. 1998; Perlmutter et al. 1999; Schmidt et al. 1998) and on Cold Dark Matter (CDM) particles as the source of structure formation processes, is far from being accepted as a satisfactory description of the Universe. The lack of a firm physical interpretation of the two main dark constituents of the cosmic energy budget, Dark Energy (DE) and CDM, represents in fact an open issue that is presently motivating an enormous effort in the community both concerning

the development of alternative theoretical models and the implementation of observational tests capable to falsify the standard scenario.

Furthermore, the severe fine-tuning problems that characterize the cosmological constant (see e.g. Weinberg 1989) and the increasing number of astrophysical observations suggesting a possible tension with the predictions of the Λ CDM paradigm (see e.g. Boylan-Kolchin et al. 2011; Lee & Komatsu 2010; Thomas et al. 2011; Lovell et al. 2011) have stimulated the development of a wide variety of alternative scenarios. These range from simple dynamical DE models based on a minimally coupled scalar field as e.g. *Quintessence* (Wetterich 1988; Ratra & Peebles

1988) or *k-essence* (Armendariz-Picon et al. 2001) to interacting DE models (Wetterich 1995; Amendola 2000), to modifications of General Relativity at cosmological scales (see e.g. Hu & Sawicki 2007), Warm Dark Matter scenarios (Bode et al. 2001), or Clustering DE models (Creminelli et al. 2010). All these models should therefore be tested by a direct comparison of their characteristic features with observations. This requires to develop accurate predictions of the effects of all these different scenarios on various observable quantities, from the background evolution down to the highly nonlinear regime of cosmic structure formation

In the next decade, a large number of observational ventures, such as the ESA approved EUCLID¹ mission (Laureijs et al. 2011), will enormously improve the constraints on the minimal set of parameters that characterize the standard Λ CDM cosmological scenario. However, the quest for a physical interpretation of the dark components of the Universe demands for an extension of these observational probes beyond such minimal parameters set, allowing for a richer phenomenology of the dark sector with respect to what envisaged by the standard model. In fact, although clearly necessary, the continuous improvement of the observational constraints on the standard cosmological parameters might not be sufficient to detect possible failures of the Λ CDM scenario, thereby preventing a deeper understanding of the physical properties of the dark universe. This is mainly due to the fact that the observable deviations from the expectations of the standard model are in many cases totally or partially degenerate with one or more of the standard cosmological parameters, which makes it particularly difficult to disentangle the two effects.

It is therefore a crucial task for a full exploitation of present and future observational probes to investigate to which extent the characteristic features of a wide range of alternative cosmological scenarios might be hidden beyond a simple shift in one or more of the standard Λ CDM cosmological parameters. In particular, in the present paper we will study in great detail the halo mass function (hereafter HMF) of groups and clusters of galaxies in the context of a significant number of interacting Dark Energy scenarios and we will investigate their apparent degeneracy with the amplitude of linear density perturbations encoded by the power spectrum normalization σ_8 . Indeed, a precise calibration of the HMF represents the basic ingredient to exploit the potential of galaxy clusters as tracers of cosmic growth (see e.g., Allen et al. 2011, for a recent review).

Within the standard Λ CDM paradigm, a number of HMF studies have been carried out through the years, based on N-body simulations covering progressively larger dynamic ranges, with the purpose of calibrating fitting functions for a universal HMF (e.g. Sheth & Tormen 1999; Jenkins et al. 2001; Reed et al. 2003; Warren et al. 2006; Lukić et al. 2007), or to characterize subtle deviations from this universality (e.g. Reed et al. 2007; Tinker et al. 2008; Crocce et al. 2010). Extensions of these studies to include the effect of baryons on the HMF have been made possible only recently by the advent of cosmological hydrodynamical simulations covering an adequate range of halo masses

(Rudd et al. 2008; Stanek et al. 2009; Cui et al. 2011). It is however clear that the quest of exploring cosmological models beyond the standard one, requires enlarging the range of models for which the HMF calibration needs to be carried out, and whose universality with respect to variations of the parameters relevant for each specific class of models needs to be assessed. For instance, Bhattacharya et al. (2011) analyzed the HMF for an extended suite of simulations of quintessence models, and confirmed violation of universality at the ~ 10 per cent level for the range of masses and redshift covered by their simulations.

A semi-analytic study of the HMF for coupled DE models has been recently carried out by Tarrant et al. (2011). Using the expressions for a universal Λ CDM HMF, they computed the variations in the cluster counts induced by the modification in the spherical collapse model induced by the DE coupling to CDM.

In this paper, we make use of the publicly available catalogs of the CoDECS² N-body simulations (Baldi 2011c), to analyse in detail the effect that different coupled DE models have on the evolution of the HMF. We will directly compare the number counts of massive halos identified both through a Friend-of-Friend (FoF) algorithm and through a Spherical Overdensity (SO) algorithm at different overdensities with the standard fitting functions calculated assuming different values of σ_8 . Former analysis of the HMF for N-body simulations of Coupled DE models were presented in Baldi et al. (2010) and Baldi (2011d). Their analysis, which was based on simulations covering a narrower dynamic range and parameter space than those analysed here, and only considered halos identified from the FoF algorithm, showed that HMF in Coupled DE models can be described well by the Λ CDM HMF after suitably rescaling σ_8 . This implied that the signature of coupling in the observational analysis of the cluster mass function could be completely masked by a modified power spectrum normalization. In our analysis we will verify whether this degeneracy between DE coupling and power spectrum normalization can be broken at the level of accuracy allowed by these simulations, by following the redshift evolution of the HMF.

The paper is organized as follows. In Section 2 we describe the Coupled DE models considered in our analysis. Section 3 is devoted to the description of the corresponding simulations and to the halo identification procedure. In Section 4 we will present the results of our analysis of the HMF and their interpretation in terms of variation of halo concentration induced by the presence of the DE coupling. We will summarize our main results and draw our conclusions in Section 5.

2 THE COUPLED DARK ENERGY MODELS

Interacting DE models have been widely discussed and investigated in the literature in the last years (see e.g. Amendola 2000, 2004; Farrar & Rosen 2007; Pettorino & Baccigalupi 2008; Amendola et al. 2008; Koyama et al. 2009; Honorez et al. 2010; Baldi 2011d;

¹ <http://www.euclid-ec.org/>

² <http://www.marcobaldi.it/web/CoDECS.html>

Model	Potential	α	β_0	β_1	$w_\phi(z=0)$	$\sigma_8(z=0)$
Λ CDM	$V(\phi) = A$	–	–	–	–1.0	0.809
EXP001	$V(\phi) = Ae^{-\alpha\phi}$	0.08	0.05	0	–0.997	0.825
EXP002	$V(\phi) = Ae^{-\alpha\phi}$	0.08	0.1	0	–0.995	0.875
EXP003	$V(\phi) = Ae^{-\alpha\phi}$	0.08	0.15	0	–0.992	0.967
EXP008e3	$V(\phi) = Ae^{-\alpha\phi}$	0.08	0.4	3	–0.982	0.895
SUGRA003	$V(\phi) = A\phi^{-\alpha}e^{\phi^2/2}$	2.15	–0.15	0	–0.901	0.806

Table 1. The list of cosmological models considered in the CoDECS project and their specific parameters.

Tarrant et al. 2011; Clemson et al. 2011) and a new detailed presentation of these cosmological scenarios would be superfluous in the present paper. We therefore refer the interested reader to the above mentioned literature for a thorough description of coupled DE (cDE) models and for the derivation of their main equations. We limit our discussion here to the definition of the notation and of the conventions adopted for the specific cDE models considered in our analysis.

In the present paper, we will consider the set of cDE models presently included in the CoDECS suite of N-body simulations (Baldi 2011c) – the largest set of cosmological simulations to date for interacting DE cosmologies – that have been presented and discussed in Baldi (2011b) and Baldi (2011c). These are flat cosmological models where the role of DE is played by a dynamical scalar field ϕ with a self-interaction potential $V(\phi)$ exchanging energy-momentum with the CDM fluid through an interaction term defined by the following set of equations:

$$\ddot{\phi} + 3H\dot{\phi} + \frac{dV}{d\phi} = \sqrt{\frac{2}{3}}\beta_c(\phi)\frac{\rho_c}{M_{\text{Pl}}}, \quad (1)$$

$$\dot{\rho}_c + 3H\rho_c = -\sqrt{\frac{2}{3}}\beta_c(\phi)\frac{\rho_c\dot{\phi}}{M_{\text{Pl}}}, \quad (2)$$

$$\dot{\rho}_b + 3H\rho_b = 0, \quad (3)$$

$$\dot{\rho}_r + 4H\rho_r = 0, \quad (4)$$

$$3H^2 = \frac{1}{M_{\text{Pl}}^2}(\rho_r + \rho_c + \rho_b + \rho_\phi), \quad (5)$$

where the subscripts b , c , and r indicate the baryonic, CDM, and radiation components of the universe, respectively. In Eqs. (1-5) an overdot represents a derivative with respect to the cosmic time t , $H \equiv \dot{a}/a$ is the Hubble function, and $M_{\text{Pl}} \equiv 1/\sqrt{8\pi G}$ is the reduced Planck mass. The source terms at the right hand side of Eqs. (1,2) represent the interaction between DE and CDM, where the dimensionless coupling function $\beta_c(\phi)$ sets the coupling strength while the sign of the quantity $\beta_c(\phi)\dot{\phi}$ defines the direction of the energy-momentum flow between the two components. The energy exchange determines a time variation of the CDM particle mass, according to the equation:

$$\frac{d \ln M_c}{dt} = -\sqrt{\frac{2}{3}}\beta_c(\phi)\dot{\phi}, \quad (6)$$

which can be derived from Eq. (2).

In the present work, we will consider two possible choices for the coupling function $\beta_c(\phi)$, defined as:

$$\beta_c(\phi) = \beta_0 e^{\beta_1 \phi}, \quad (7)$$

namely a constant coupling ($\beta_1 = 0$) and an exponen-

tially growing coupling ($\beta_1 > 0$). The latter case, first proposed by Amendola (2004) and subsequently investigated by Baldi (2011d), allows for larger values of the present coupling strength β_0 as compared to constant coupling models, since the impact of the interaction on the background expansion history of the universe and on the Cosmic Microwave Background anisotropies is strongly suppressed by the time evolution of the scalar field ϕ . Furthermore, we will consider two distinct choices also for the scalar self-interaction potential $V(\phi)$, namely an exponential potential (Lucchin & Matarrese 1985; Wetterich 1988; Ferreira & Joyce 1998):

$$V(\phi) = Ae^{-\alpha\phi} \quad (8)$$

and a SUGRA potential (Brax & Martin 1999):

$$V(\phi) = A\phi^{-\alpha}e^{\phi^2/2}, \quad (9)$$

where for simplicity the field ϕ has been expressed in units of the reduced Planck mass in Eqs. (8,9). The main phenomenological difference between these two potential functions resides in the existence of a global minimum at a finite ϕ value for the SUGRA potential, while the exponential potential is monotonically decreasing to zero for $\phi \rightarrow \infty$. The presence of a global minimum in the SUGRA potential allows for an inversion of the scalar field motion and for a consequent change of sign – in case of a constant coupling β_c – of the quantity $\beta_c\dot{\phi}$, as discussed in Baldi (2011b) (see also Tarrant et al. 2011). Due to such inversion, the DE equation of state parameter $w_\phi \equiv p_\phi/\rho_\phi$ shows a “bounce” on the cosmological constant “barrier” $w_\phi = -1$, for which this class of models has been dubbed the “Bouncing cDE scenario” (Baldi 2011b). For the specific model considered in the present work, the “bounce” happens at relatively recent epochs, $z_{\text{inv}} \approx 6.8$, and has significant consequences on the evolution of linear and nonlinear perturbations (see again Baldi 2011b). The effect of the coupling on the background evolution of the universe is to allow for a phase of Early Dark Energy which goes under the name of ϕ -MDE (ϕ -Matter Dominated Epoch, see Amendola 2000) or G- ϕ -MDE (Growing- ϕ -Matter Dominated Epoch, see Baldi 2011d) for models with constant and variable couplings, respectively. Such scaling behavior of the DE density determines a different expansion history of cDE models with respect to a Λ CDM cosmology with the same cosmological parameters, which represents one of the most characteristic features of cDE scenarios and that is correctly taken into account in the numerical implementation of the CoDECS simulations described in the next Section. All the features and the parameters of the different models

investigated in the present work are summarized in Table 1.

The effect of the coupling on the growth of linear density perturbations is described by the evolution equations for linear fluctuations $\delta_{b,c}$ for baryons and CDM, respectively (see e.g. Amendola 2004; Pettorino & Baccigalupi 2008):

$$\ddot{\delta}_c = -2H \left[1 - \beta_c \frac{\dot{\phi}}{H\sqrt{6}} \right] \dot{\delta}_c + 4\pi G [\rho_b \delta_b + \rho_c \delta_c \Gamma_c], \quad (10)$$

$$\ddot{\delta}_b = -2H \dot{\delta}_b + 4\pi G [\rho_b \delta_b + \rho_c \delta_c], \quad (11)$$

where for simplicity the field dependence of the coupling function $\beta_c(\phi)$ has been omitted. The factor Γ_c is defined as $\Gamma_c \equiv 1 + 4\beta_c^2(\phi)/3$ and represents a fifth-force acting on CDM perturbations, while the term $2\beta_c(\phi)\dot{\phi}/\sqrt{6}$ is an extra-friction arising as a consequence of momentum conservation. The combination of these two effects determines the deviation of the evolution of linear density perturbations from the standard Λ CDM case. At the nonlinear level, the same two extra terms appear in the acceleration equation of coupled particles (see Baldi et al. 2010, for a derivation of the acceleration equation):

$$\dot{\mathbf{v}}_c = \beta_c(\phi) \frac{\dot{\phi}}{\sqrt{6}} \mathbf{v}_c - \nabla \left[\sum_c \frac{GM_c(\phi)\Gamma_c}{r_c} + \sum_b \frac{GM_b}{r_b} \right], \quad (12)$$

where $r_{c,b}$ is the physical distance of the target coupled particle from the other CDM and baryonic particles, respectively. However, in this case the relative orientation of the particle’s velocity \mathbf{v}_c and of the local gradient of the gravitational potential $\nabla\Phi$ introduces an additional degree of freedom and plays an important role in the evolution of nonlinear structures in the context of cDE scenarios (see Baldi 2011a, for a detailed discussion of nonlinear effects in cDE models).

Clearly, for any chosen coupling $\beta_c(\phi)$ and potential slope α in a cDE model, it is always possible to reconstruct an effective equation of state $w_{\text{eff}}(z)$ for a minimally coupled scalar field cosmology that provides the same expansion history. In this respect, the specific background evolution of any cDE model does not represent a “smoking gun” capable to uniquely identify the presence of an interaction in the dark sector, as the same expansion history might be provided by a suitably tuned standard *Quintessence* or *phantom* DE fluid. On the other hand, any pair of cDE models with different coupling functions but with identical cosmological parameters at $z = 0$ (except for the value of the equation of state) will necessarily have different background expansion histories due to their different ϕ -MDE scaling solutions in matter domination (since the energy fraction of the Early Dark Energy component during ϕ -MDE is proportional to $\beta^2(\phi)$, see e.g. Amendola 2000; Baldi 2011d). Therefore, in order to investigate solely the impact of the DE-CDM coupling on the growth of structures one would need to compare any given cDE model with a specific standard *Quintessence* or *phantom* DE scenario having the same expansion history. However, this would necessarily imply to choose a different reference model for every different coupling function $\beta(\phi)$. In our study, instead, we are interested in comparing a range of different cDE models with one single minimally coupled reference scenario, given by the concordance Λ CDM cosmology, all having the same WMAP7 parameters at $z = 0$, by including all the effects (i.e. modified background expan-

Parameter	Value
H_0	70.3 km s ⁻¹ Mpc ⁻¹
Ω_{CDM}	0.226
Ω_{DE}	0.729
σ_8	0.809
Ω_b	0.0451
n_s	0.966

Table 2. Parameters of the reference Λ CDM model which is used to generate initial conditions for all the cDE simulations (see text).

sion history, enhanced growth of linear density perturbations, particle mass variation, and scalar fifth-force).

3 THE SIMULATIONS AND HALO IDENTIFICATION

3.1 The N-body simulations

For our analysis we will make use of the public data of the CoDECS simulations (Baldi 2011c) – the largest suite of cosmological simulations to date for cDE cosmologies – which include all the specific models listed in Table 1. The public data of the CoDECS project have already been used to investigate the characteristic features of cDE scenarios in terms of z -space distortions (Marulli et al. 2011), of the expected Weak Lensing signatures (Beynon et al. 2011) and of the abundance of “Bullet-like” systems (Lee & Baldi 2011).

In the present work, we will consider in particular the L-CoDECS runs, that follow the evolution of 1024^3 CDM and 1024^3 baryon particles in a periodic cosmological box of 1 comoving h^{-1} Gpc aside. The simulations have been carried out with the modified version by Baldi et al. (2010) of the widely used parallel TreePM N-body code GADGET (Springel 2005), which implements all the specific features of cDE models described in Sec. 2. The L-CoDECS simulations have a mass resolution at $z = 0$ of $m_c = 5.84 \times 10^{10} h^{-1} M_\odot$ for CDM and $m_b = 1.17 \times 10^{10} h^{-1} M_\odot$ for baryons.

In order to cover a large dynamic range over which to study the effect of coupled DE with an affordable computational cost, our simulations account for the different forces acting on the uncoupled DM and coupled baryonic matter components, without including the hydrodynamic description of baryons. As such, our simulations are designed to follow the evolution of two populations of collisionless particles, which feel different gravitational forces. We refer to the analyses by Rudd et al. (2008); Stanek et al. (2009); Cui et al. (2011) for discussions on the effect of hydrodynamics on the HMF.

Initial conditions for all the simulations have been generated by perturbing a homogeneous “glass” particle distribution (White 1994; Baugh et al. 1995) according to Zel’dovich approximation (Zel’dovich 1970) in order to produce a random-phase realization of the same initial matter power spectrum, corresponding to the one computed by the public Boltzmann code CAMB (Lewis et al. 2000) for a Λ CDM cosmology with parameters consistent with the “WMAP7 only Maximum Likelihood” results of Komatsu et al. (2011), which are listed in Table 2.

Since the same random seed has been adopted for the initial conditions generation of all the L-CoDECS runs, all the different cosmological models share exactly the same particle displacements at $z_{\text{CMB}} \approx 1100$. The initial conditions for each specific simulation are realized by scaling such displacements to the starting redshift of the numerical integration $z_1 = 99$ with the specific growth function obtained by numerically solving Eqs. (10,11) for each individual cosmology.

3.2 The Halo Identification

The two most common methods for halo identification in N-body simulations are based on the Friend-of-Friend (FoF) algorithm (e.g. Davis et al. 1985) and on the spherical overdensity (SO) algorithm (e.g. Lacey & Cole 1994). The FoF halo finder has only one parameter, b , which defines the linking length λ as $\lambda \equiv b \cdot l$, where $l = n^{-1/3}$ is the mean inter-particle separation, with n the mean particle number density. In the SO algorithm there is also only one free parameter, namely the mean density $\Delta_c \rho_{\text{crit}}(z)$ contained within the sphere over which the halo mass is computed, with $\rho_{\text{crit}}(z)$ being the critical cosmic density at redshift z . Note that our definition of the spherical overdensity Δ_c is given with respect to the critical density ρ_{crit} instead of the background matter density ρ_{mean} , which means that our Δ_c is Ω_m times the commonly used overdensity parameter Δ . Each of the two halo finders has its own advantages and shortcomings (see more details in Jenkins et al. 2001; White 2001; Tinker et al. 2008, and references therein). The difference of halo mass and HMF resulting from the two methods have been discussed in several analysis (see e.g. White 2002; Reed et al. 2003, 2007; Cohn & White 2008; More et al. 2011).

In this paper, we applied both methods to identify halos and to compare the respective HMF for the CoDECS set of N-body simulations. First, the standard FoF algorithm has been applied, with a linking parameter $b = 0.2$, only over the CDM particles in the simulations as primary tracers of the matter distribution. Subsequently, each baryonic particle has been attached to the FoF group of its closest CDM neighbor. The gravitationally bound substructures of each FoF halo have also been identified by means of the SUBFIND algorithm (see more details in Springel et al. 2001; Dolag et al. 2009). The position of the most bound particle of each substructure defines then the center of the subhalo.

As a second step, the SO halo catalogues are built using a fast SO algorithm (see also Cui et al. 2011). In this SO algorithm, the centers of spherical regions are identified with the positions of the most bound particles within the main subhalo of each FoF group, as identified by SUBFIND. Meanwhile, the region encompassed by R_{200} (i.e. the spherical region enclosing a mean overdensity 200 times larger than the critical density) around each FoF halo is also checked, and all the substructures identified by SUBFIND, that lie outside this region, are considered as new independent FoF groups. The most bound particle of each such new independent halos is then used again as the center of a new SO region. For each independent halo identified with this method we progressively increase the radius of a sphere centered on the most bound particle until a specified mean internal density contrast $\Delta_c \rho_{\text{crit}}(z)$ is reached. The mass M_{Δ_c} within this

spherical region of radius R_{Δ_c} is then

$$M_{\Delta_c} = \frac{4}{3}\pi R_{\Delta_c}^3 \Delta_c \rho_{\text{crit}}(z). \quad (13)$$

Since each halo is firstly identified starting from a FoF algorithm, it inherits some FoF disadvantages. A well known potential problem with FoF is that there are situations in which two halos are connected through a bridge of particles. Our check of all the substructures lying outside R_{200} should reduce this effect, especially for the most massive halos. As discussed by Reed et al. (2007), this effect becomes more important at high redshift and for poorly resolved low-mass halos. Since our analysis mainly concentrates on very massive halos, which we select to be resolved by at least 200 particles, we expect the bias induced by using FoF parent groups to be relatively small. In order to verify this on a few test cases, we also used the SUBFIND results to check the mass ratio of all the subhalos within each FoF group, with respect to the main halo. Whenever a prominent subhalo is found whose mass is at least 0.7 times the mass of the main halo, we treat it as a distinct halo. We verified that such halos are extremely rare after we remove subhalos lying outside R_{200} , at least over the mass range $M \gtrsim 10^{13} h^{-1} M_{\odot}$ considered in our analysis, so our results are not influenced by this effect. Finally, since the groups identified by the FoF algorithm have by definition no overlapping, we do not include in our identification of SO halos any restriction to prevent such overlapping (see Tinker et al. 2008 for a discussion on halo overlapping).

We do not apply the commonly used FoF mass correction of Warren et al. (2006) for our FoF halos in this paper. This correction is meant to regulate the halo mass, which is overestimated by the FoF algorithm when halos are sampled with too few particles. This correction is expected to be small for our selected halo sample, due to the minimum threshold of 200 particles per halo that we adopted.

4 RESULTS

Under simplifying assumptions, Press & Schechter (1974) were the first to provide a theoretical description for the abundance of collapsed halos as a function of their mass. Thanks to the calibration on N-body simulations covering wide dynamic ranges, the HMF for the standard Λ CDM cosmology can now be accurately described by analytical models and fitting functions, as provided by e.g. Sheth & Tormen (1999); Jenkins et al. (2001); Reed et al. (2003); Warren et al. (2006); Tinker et al. (2008). In most applications, the HMF is expressed in terms of the so-called multiplicity function by:

$$f(\sigma, z) = \frac{M}{\rho_0(z)} \frac{dn(M, z)}{d \ln \sigma^{-1}(M, z)}, \quad (14)$$

where $n(M, z)$ is the number density of halos with mass M at redshift z and $\rho_0(z)$ is the background density at redshift z . In Eq. (14), $\sigma^2(M, z)$ is the variance of the linear density field, extrapolated to the redshift z at which halos are identified, which is given by

$$\sigma^2(M, z) = \frac{D^2(z)}{2\pi^2} \int_0^{\infty} k^2 P(k) W^2(k, M) dk. \quad (15)$$

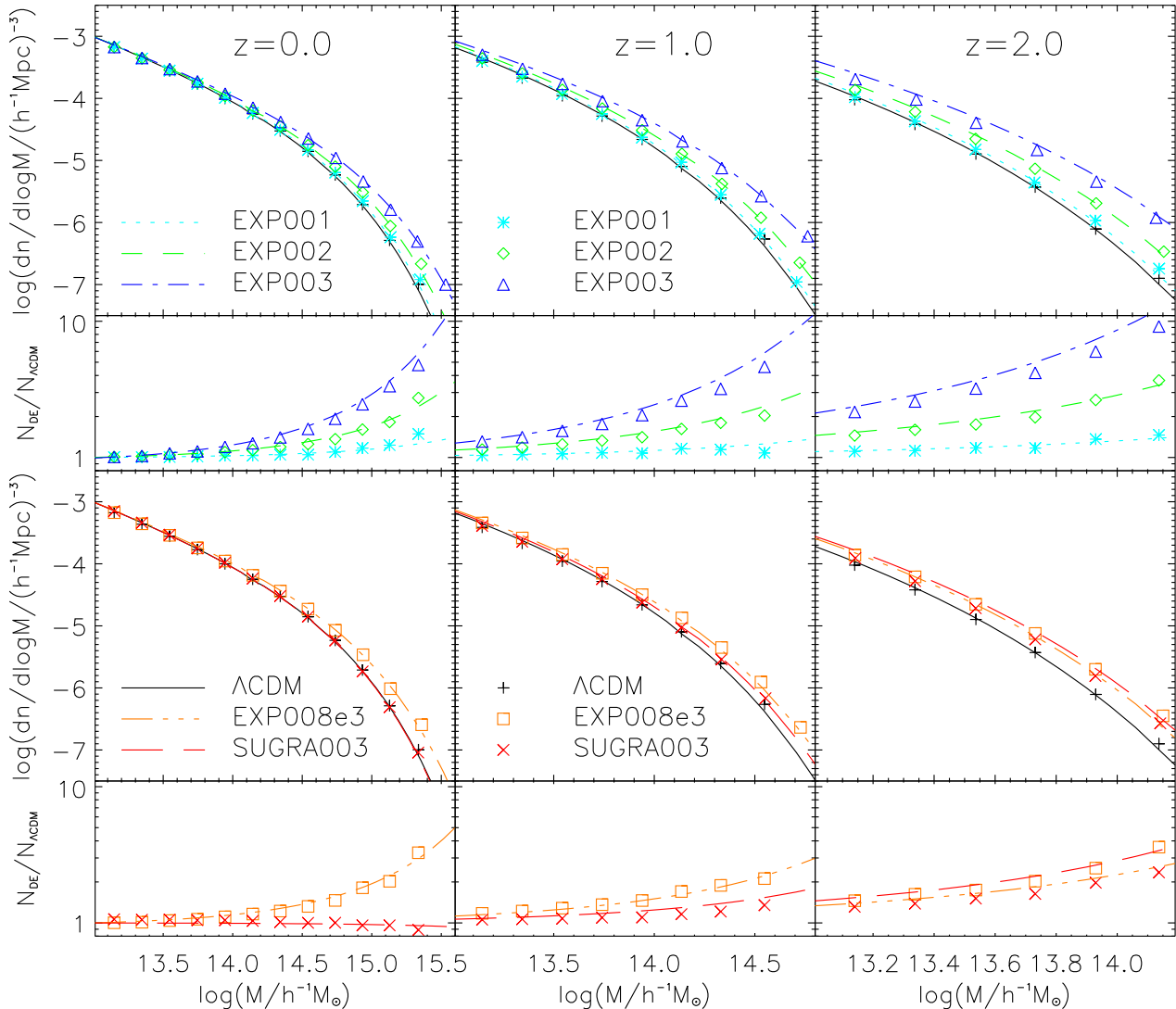


Figure 1. The FoF halo mass function (HMF) for the different cDE simulations at $z = 0, 1$ and 2 (left, central and right panels, respectively). In all cases $b = 0.2$ is assumed for the linking parameter used in the FoF halo identification. In the upper part of each panel the symbols show the results from our simulations, while curves are the corresponding predictions from the FoF HMF of Eq. 17 calibrated by Jenkins et al. (2001) for a Λ CDM cosmology and rescaled to the value of σ_8 appropriate for each cDE model. In all panels, black crosses and black curves are for the results of our Λ CDM reference simulation. The lower part of each panel shows the difference with respect to Λ CDM results. Here symbols show the difference between cDE and Λ CDM simulations, while curves with different line-styles show the difference between the corresponding fitting functions.

In Eq. (15), $D(z)$ is the growth factor of linear density perturbations, $P(k)$ is the linear power spectrum of density perturbations and $W(k, M)$ is the Fourier-space representation of a real-space top-hat filter of radius R , which on average encloses a mass $M = 4\pi R^3 \rho_0(z)/3$, given by:

$$W(k, R) = \frac{3}{(kR)^3} [\sin(kR) - kR \cos(kR)]. \quad (16)$$

Using a series of N-body simulations under the standard Λ CDM cosmology and applying the FoF algorithm with linking parameter $b = 0.2$, Jenkins et al. (2001) (J01 hereafter) provided a simple fitting formula as a function of the variance σ , which is independent of redshift:

$$f(\sigma) = 0.315 \exp(-|\ln \sigma^{-1} + 0.61|^{3.8}). \quad (17)$$

This fitting function is valid over the range $-1.2 \leq \ln \sigma^{-1} \leq 1.05$, which corresponds to halo masses $10.3 \leq \log(M/h^{-1} M_\odot) \leq 15.6$ in our Λ CDM simulation. We use this formula as our benchmark reference fit for the FoF HMF. We adopt instead the fitting function of Tinker et al. (2008) (T08 hereafter) for the SO HMF. This fitting function $f(\sigma)$ is tuned by the four parameters A, a, b, c according to:

$$f(\sigma) = A \left[\left(\frac{\sigma}{b} \right)^{-a} + 1 \right] e^{-c/\sigma^2}. \quad (18)$$

These four parameters are functions of two independent variables, namely the redshift z and the overdensity Δ (for more details, see Eqs. 5–7 and B1–B4 in T08). As already mentioned, T08 adopted an overdensity Δ computed with re-

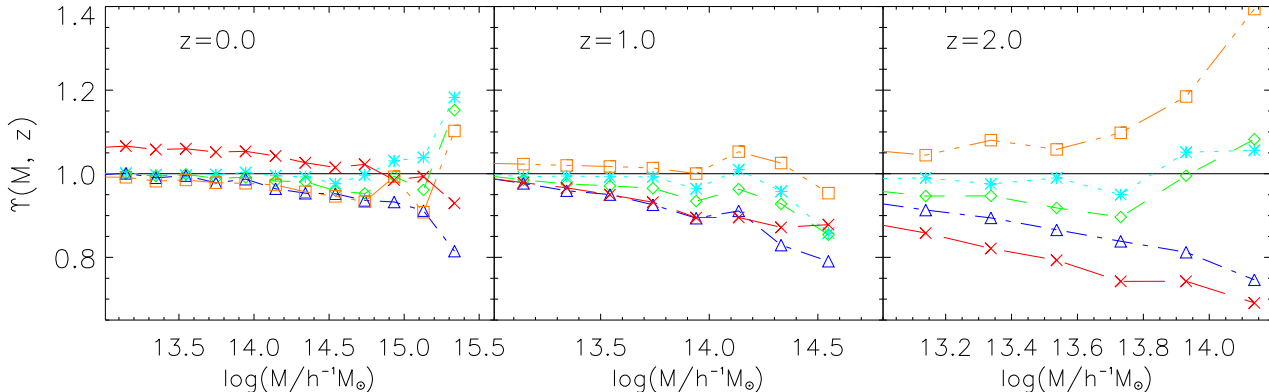


Figure 2. The ratio between the FoF halo counts in different mass intervals from the cDE models and from the reference Λ CDM model from simulations, compared to the same quantity computed from the corresponding fitting functions from Eq. 21 (see also text). Deviations of this quantity from unity indicates that simply rescaling σ_8 in the fitting function of Eq.17 does not correctly account for the difference between cDE and Λ CDM simulation results. The correspondence of simulated models with symbols and line-types is the same as in Fig. 1.

spect to the background matter density. In order to use this fitting function with our definition of the overdensity Δ_c (i.e. with respect to the critical density of the Universe), we simply change Δ to Δ_c in the functional dependence of the four parameters (A, a, b, c) just multiplying it by $\Omega_m(z)$.

Throughout this paper, we adopt the differential HMF $dn/d\log M$ to make comparisons between theoretical predictions and simulation results. With a simple transformation of Eq. (14), the theoretical expression for $dn/d\log M$ is given by:

$$\frac{dn}{d\log M} = \frac{f(\sigma)\rho_0}{M} \frac{d\ln\sigma^{-1}}{d\log M}, \quad (19)$$

where $f(\sigma)$ is given by Eqs. (17) and (18).

In order to compute the differential HMF $dn/d\log M$ in a simulation of volume L^3 , one needs to measure the number of halos ΔN in a given logarithm mass bin $\Delta\log M$:

$$\frac{dn}{d\log M} = \frac{M}{L^3} \frac{\Delta N}{\Delta\log M}, \quad (20)$$

where we assigned the characteristic mass M for a given mass bin as the mean mass computed over all halos belonging to that bin. For our halo sample, we used narrow mass bins with $\Delta\log M = 0.2$. Lukić et al. (2007) had studied the error introduced by binning data, and showed that this error is negligible with such a narrow bin. However, the limited statistics of high-mass halos within the simulation box makes the determination of the HMF quite noisy in the high mass end, especially when narrow mass bins are used. To reduce this effect, we merge mass bins containing less than 20 objects into the adjacent lower mass bin. Each mass bin is then weighted proportionally to the number of clusters it contains. Due to this specific treatment of the mass bins at large masses, the bin width can be different for different simulations. Therefore, when we compare the number of objects in such last bins, we rescale the cluster counts within each of them to the bin width in units of $\Delta\log M = 0.2$.

4.1 The FoF HMF in coupled dark energy models

We show the FoF HMF of the different cDE models included in the CoDECS project derived from the L-CoDECS simulations in the upper panels of Fig. 1. Here, the symbols show the results from simulations, while the different line-styles represent the HMF predicted by the J01 fitting function given by Eq. (17) for Λ CDM cosmologies with the same σ_8 value as the different cDE realizations (see Table 1). In the lower panels of each plot of Fig. 1 we show with symbols the ratio of the halo number density of the various cDE simulations over the corresponding results for the standard Λ CDM simulation. In the same panels, the curves show the same ratio, but obtained using the model predictions from the HMF fitting functions, each computed for the appropriate value of σ_8 . In fact, since the HMF is described only by the variance of the linear density field $\sigma^2(M, z)$, the HMF fitting functions of the Λ CDM cosmology are often assumed to predict also the HMF of other non-standard models by a simple renormalization of the linear perturbations amplitude σ_8 .

At a first sight, by looking at Fig. 1 such assumption holds also for cDE models considered in the present paper, with the predicted HMFs for the σ_8 values computed for each model through linear perturbations theory fitting the cDE simulations results reasonably well, at least at $z = 0$ (left panels). This is true for both the standard cDE models with constant coupling, EXP001-3 (upper plots), and for the other two cDE models with different potentials or coupling functions, EXP008e3 and SUGRA003 (lower plots). Quite interestingly, the accuracy of such rescaling degrades at increasing redshift, with deviations appearing at $z = 1$ (central panels), which becomes more apparent at $z = 2$ (right panels).

In order to better appreciate the difference between results from cDE simulations and fitting functions, we introduce a parameter $\Upsilon(M, z)$, which is expressed as

$$\Upsilon(M, z) = \frac{N_{DE}^{sim}(M, z)/N_{\Lambda CDM}^{sim}(M, z)}{N_{DE}^{fit}(M, z)/N_{\Lambda CDM}^{fit}(M, z)}, \quad (21)$$

where $N(M, z)$ is the number density of halos within the mass bin M at redshift z , and the lower index of N indi-

cates the model, while the upper index indicates either the theoretical (*fit*) or the simulation (*sim*) results. With this definition, the quantity $\Upsilon(M, z)$ describes the difference between simulations and fitting functions, after rescaling each to the corresponding Λ CDM prediction. In this way, we account for sampling effects, due to the limited halo statistics especially in the high-end of the simulated HMF, and for possible inaccuracies in the fitting functions. Accordingly, a significant deviation from unity of the $\Upsilon(M, z)$ parameter indicates a lack of precision in the rescaling of the HMF fitting function for the cDE models.

In Figure 2, we show the mass dependence of $\Upsilon(M, z)$ at the same redshifts considered in Fig. 1, for the different cDE models. At $z = 0$, Υ is very close to unity at small halo masses, thus implying that the J01 fitting function can be used to capture the simulation results quite accurately. The only exception is represented by the ‘‘Bouncing cDE model’’ SUGRA003 (red line), that shows a ~ 5 per cent deviation at the low-mass end of our HMF, with a decreasing trend at higher masses. Deviations from unity of the Υ parameter for this model change their sign at higher redshift, where they become progressively larger. At $z = 2$ simulation results for the SUGRA003 model show a deviation from Λ CDM simulation results that is ~ 30 per cent smaller than predicted by the corresponding J01 fitting function, for the highest sampled halo masses. An opposite trend is instead found for the variable-coupling model EXP008e3, with $\Upsilon \simeq 1.4$ for the highest masses sampled at $z = 2$. As for the standard models with constant coupling (EXP001-3), the value of Υ shows smaller deviations from unity, which also in this case increases with mass and redshift. As expected, the smallest deviations are found for the models with the smallest value of the β_0 coupling (EXP001).

In general, Figure 2 clearly shows that, even for the FoF HMF, the apparent degeneracy between the coupling and σ_8 , which holds to first approximation in the low-mass end at low redshift, is broken in the high-mass end by an amount which increases with redshift, with the strength of the coupling, and whose sign also depends on the shape of self-interaction potential for the dynamical scalar field which determines the coupling.

4.2 The SO HMF in coupled dark energy models

The FoF algorithm does not assume any geometry for the halo, unlike the enforced sphericity of SO. For this reason, the mass function for halos identified with a SO algorithms can be more directly compared with the observed mass function of galaxy clusters and groups, whose mass is generally measured, or inferred from mass proxies, within some radius encompassing a fixed overdensity Δ_c with respect to the cosmic critical density. In this section, we investigate the SO HMF at three reference overdensities $\Delta_c = 200, 500, 1500$.

In Figure 3 we show the same SO HMF properties at $\Delta_c = 200$ as shown for the FoF HMF in Figure 1 above. From the upper part of the panels of Figure 3, we see that at a first sight the SO HMF for different cDE models can also be described by a simple renormalization of σ_8 in the T08 fitting function of Eq. 18. The ratios to Λ CDM in the lower panels of Figure 3 are also qualitatively similar to what already shown for the FoF HMF in Figure 1. All the cDE models based on an exponential potential present more mas-

sive halos than Λ CDM at all the three redshifts considered, while the ‘‘Bouncing cDE model’’ SUGRA003 is consistent with Λ CDM at $z = 0$, but shows an excess of massive halos at higher redshifts, in line with the results discussed by Baldi (2011b). Also in this case, we show the Υ parameter as a function of halo mass in Figure 4. Differently from what shown for the FoF halos in Figure 2, the Υ parameter of the three standard cDE models (EXP001-3) are quite close to unity with a decline < 10 per cent at all redshifts and at all masses (except at the very high mass end). The Υ parameter for the EXP008e3 model shows an increase with redshift, which is in any case still within ~ 10 per cent. On the other hand, the Υ parameter for the SUGRA003 model is above unity, by ~ 20 – 40 per cent, at $z = 0$. Its value is larger than what shown for the FoF case of Fig. 2, while dropping below unity at $z = 2$ by ~ 10 – 20 per cent. In general, these results suggest that the σ_8 rescaling applied to the T08 fitting function provides a better fit to the SO HMF at $\Delta_c = 200$ for the standard cDE models than the same rescaling does when applied to the J01 fitting expression for the FoF HMF, except for the bouncing cDE model SUGRA003.

The SO HMFs at $\Delta_c = 500$ are shown in Figure 5. At this higher overdensity, the SO HMFs from simulations are still fit by the theoretical predictions as in Figure 3, with the ratio displayed in the lower panels also showing a similar quality of the fit as for the previous cases. From Figure 6 we see that the Υ parameter for the standard cDE models has larger deviations from unity than for the $\Delta_c = 200$ case, especially at higher redshift. As for the SUGRA003 model, this parameter is confirmed to have a decreasing trend with redshift, starting with a value at $z = 0$ which is larger than the corresponding one found for $\Delta_c = 200$.

In general, all these trends are amplified as we consider progressively larger values of Δ_c . In fact, at our highest overdensity $\Delta_c = 1500$, the fitting function by T08 does not provide a good fit to the simulation results anymore, even for the Λ CDM simulation as shown in Figure 7. Nevertheless, the ratios to corresponding Λ CDM results have a similar variation with halo mass as in the previous figures. Since the Υ parameter is the ratio between simulation and fitting-function results, rescaled to the corresponding Λ CDM predictions, it should allow to remove this offset. Figure 8 indicates that this is indeed the case, with the value of Υ still being within ~ 20 per cent from unity at $z = 0$ for all the exponential potential models, while at $z = 2$ we find deviations from unity of the order of ~ 30 per cent for the most extreme EXP003 model. On the contrary, for the SUGRA003 model Υ increases above unity by more than 60 per cent at $z = 0$, and drops to ~ 1 at $z = 2$. Some deviation from a universal shape of the HMF has been detected also for uncoupled DE scenarios based on a classical scalar field with no direct interactions to matter, as discussed by e.g. Courtin et al. (2011). However, the higher amplitude of the deviation and its peculiar mass dependence – with the effect being progressively more pronounced for halos of higher masses – make the imprint of cDE models on the HMF quite peculiar and potentially distinguishable from the one of an uncoupled model.

As a general result from the analysis of the SO HMF, we point out that rescaling the mass function in cDE models with the σ_8 value produces results that, at least for $\Delta_c = 200$, are more accurate than for the FoF HMF. However,

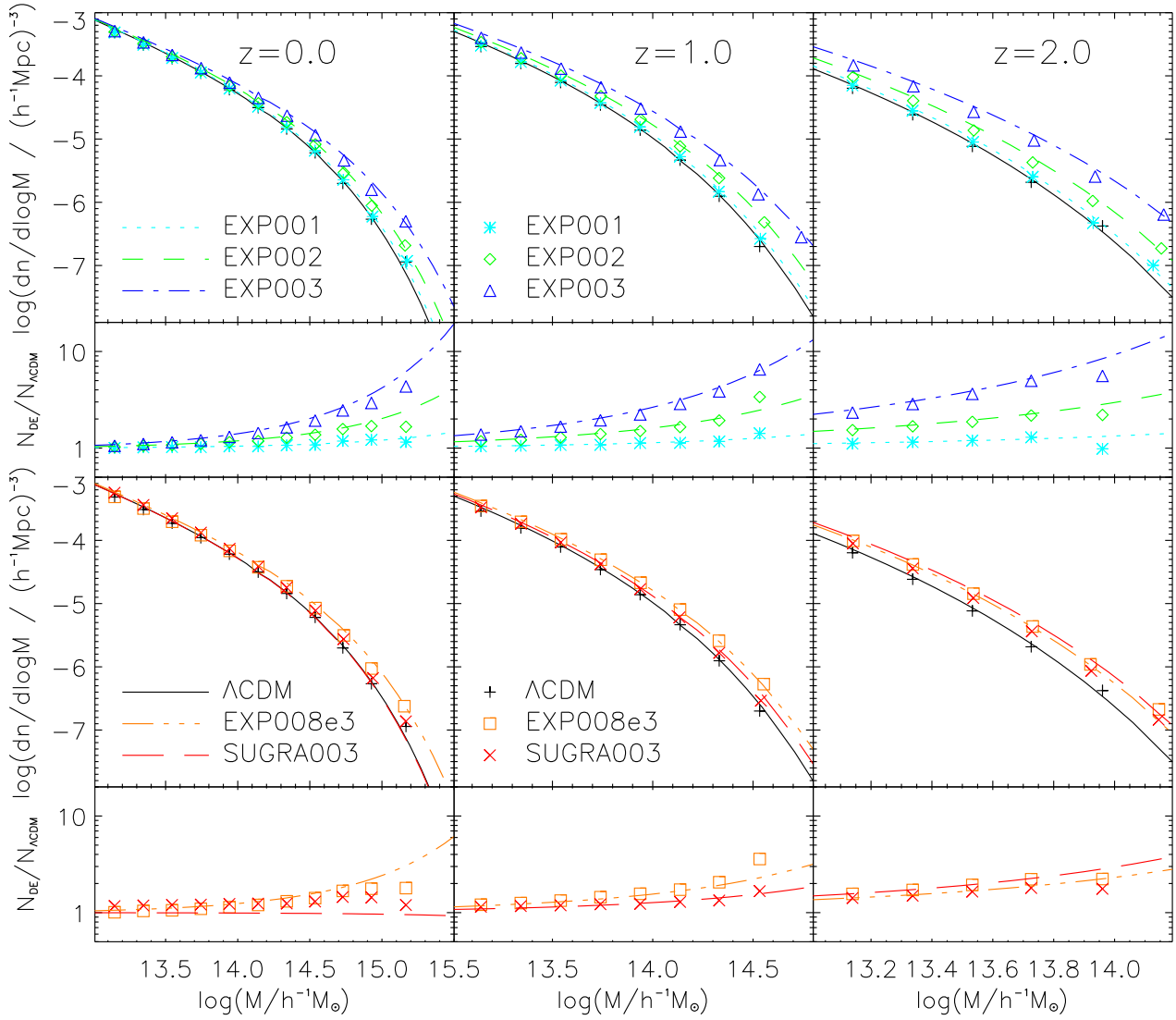


Figure 3. The same as in Figure 1, but for the HMF computed with the spherical overdensity (SO) algorithm at $\Delta_c = 200$. In this case, curves are obtained from the fitting function of Eq. 18 by Tinker et al. (2008), computed for the appropriate overdensity.

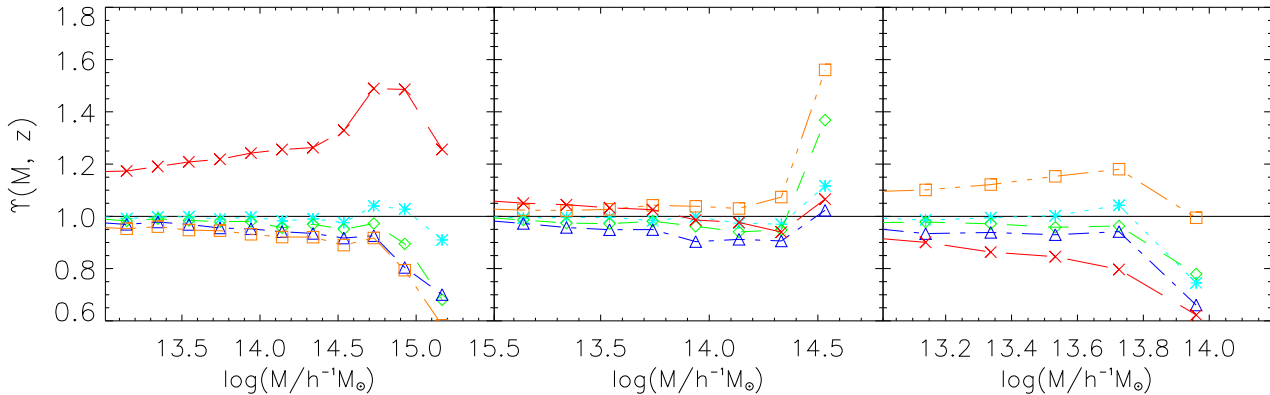


Figure 4. The same as in Figure 2, but for the HMF computed with the spherical overdensity (SO) algorithm at $\Delta_c = 200$. In this case, curves are obtained from the fitting function of Eq. 18 by Tinker et al. (2008), computed for the appropriate overdensity.

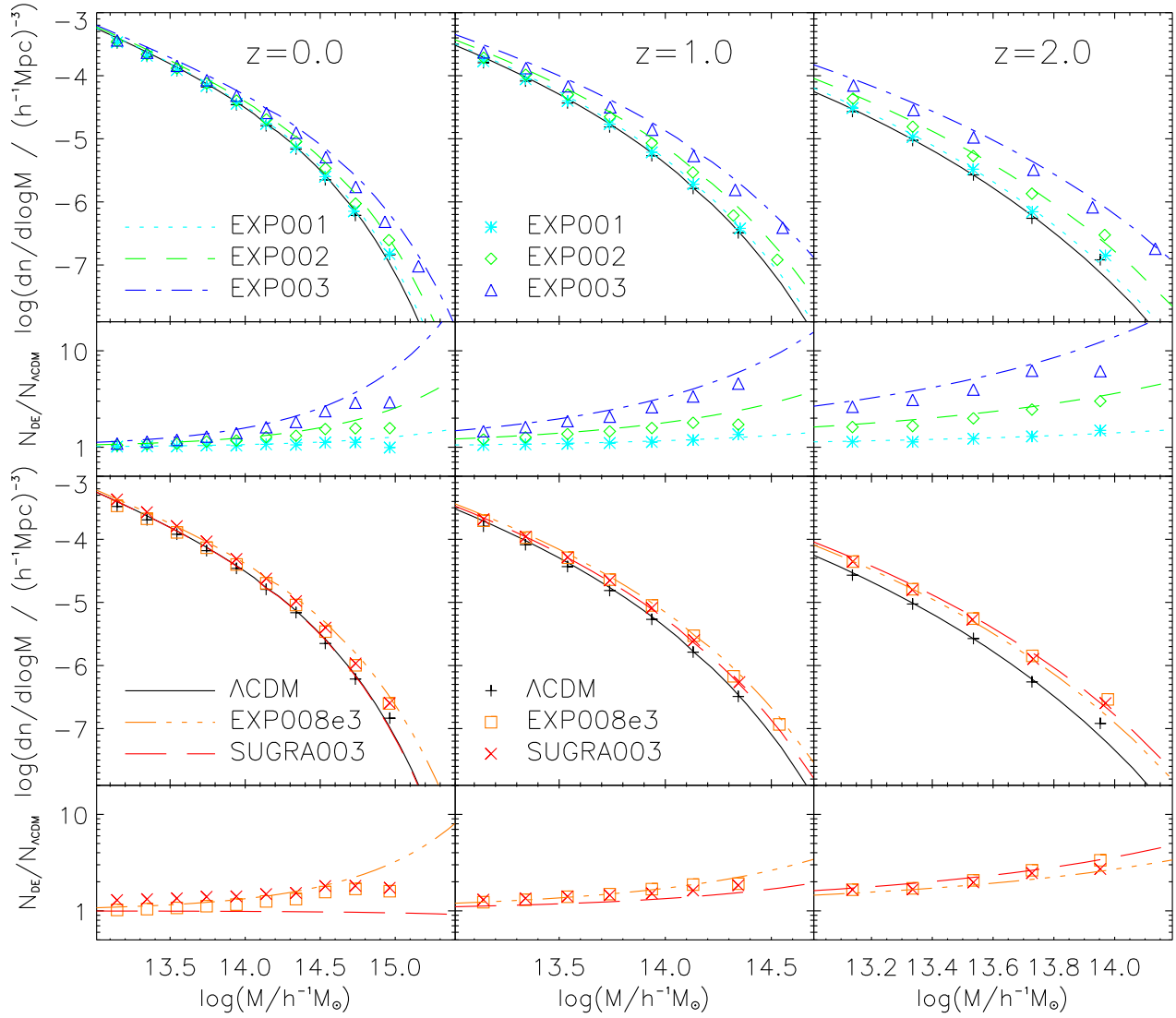


Figure 5. The same as in Figure 1, but for the HMF computed with the spherical overdensity (SO) algorithm at $\Delta_c = 500$. In this case, curves are obtained from the fitting function of Eq. 18 by Tinker et al. (2008), computed for the appropriate overdensity.

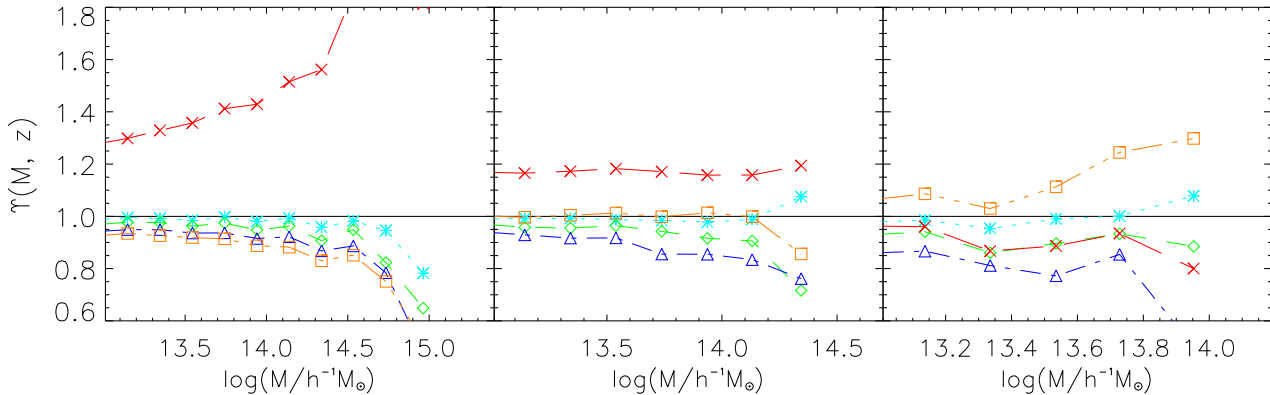


Figure 6. The same as in Figure 2, but for the HMF computed with the spherical overdensity (SO) algorithm at $\Delta_c = 500$. In this case, curves are obtained from the fitting function of Eq. 18 by Tinker et al. (2008), computed for the appropriate overdensity.

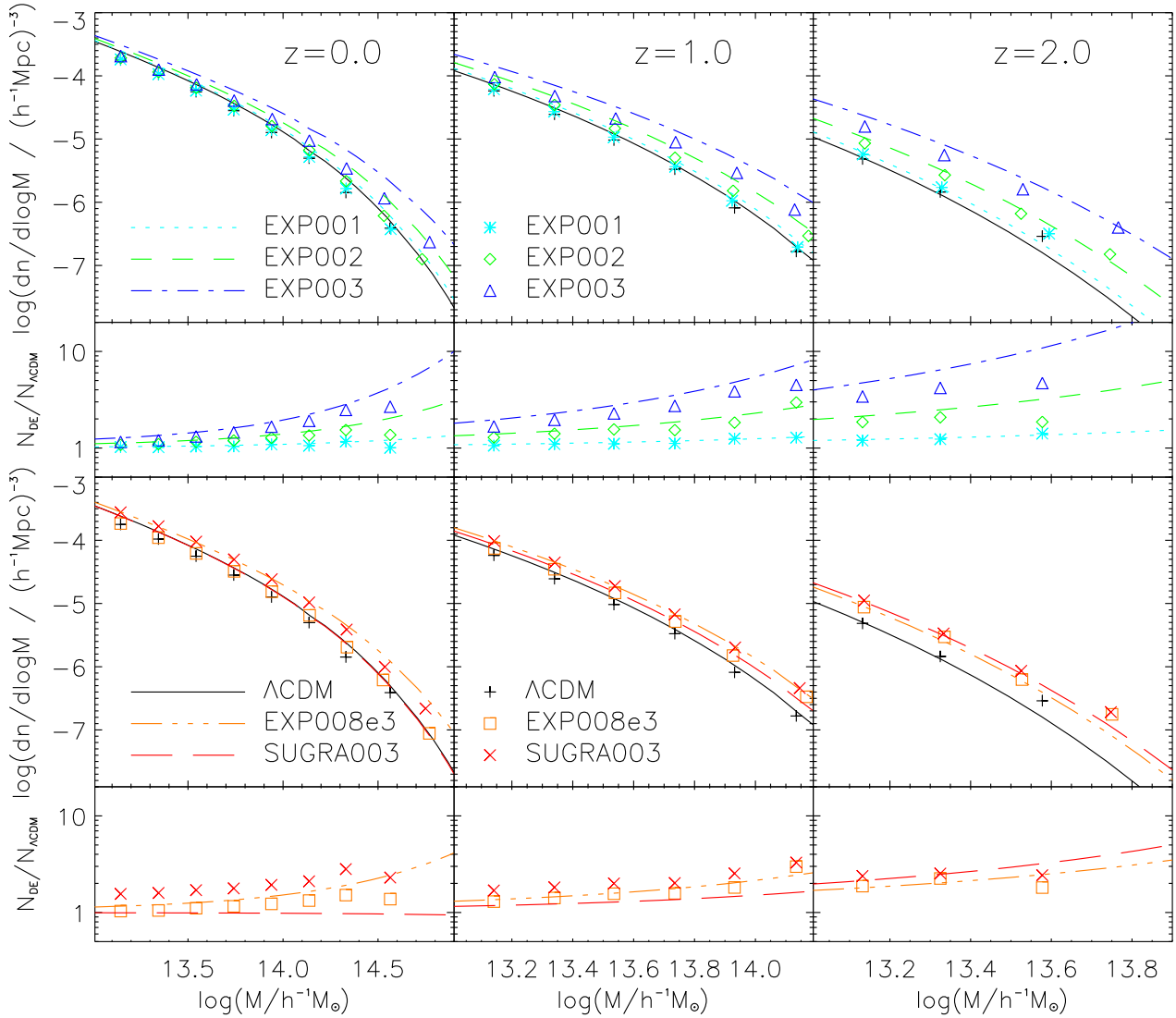


Figure 7. The same as in Figure 1, but for the HMF computed with the spherical overdensity (SO) algorithm at $\Delta_c = 1500$. In this case, curves are obtained from the fitting function of Eq. 18 by Tinker et al. (2008), computed for the appropriate overdensity.

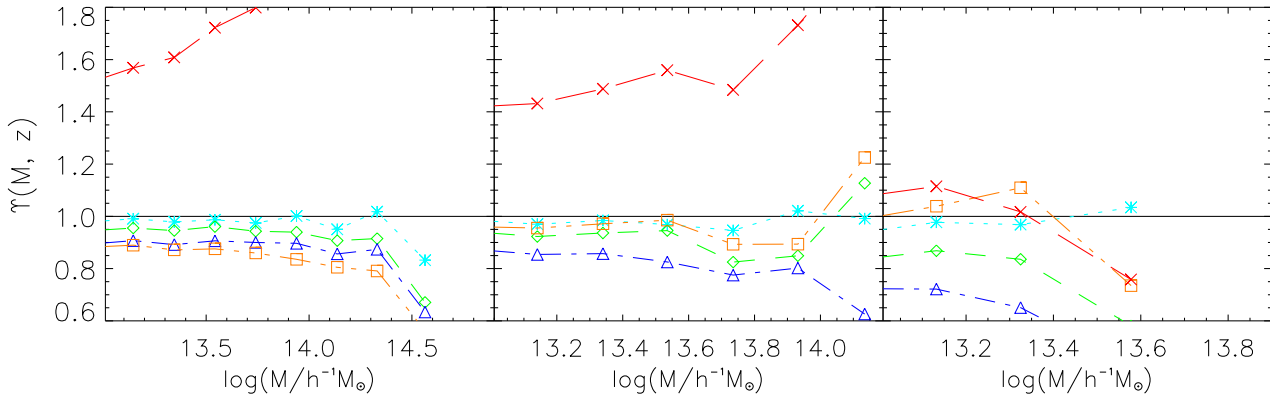


Figure 8. The same as in Figure 2, but for the HMF computed with the spherical overdensity (SO) algorithm at $\Delta_c = 1500$. In this case, curves are obtained from the fitting function of Eq. 18 by Tinker et al. (2008), computed for the appropriate overdensity.

this rescaling does not provide accurate predictions of the cDE HMF at higher overdensity and larger redshift. These results highlight that degeneracy between a non-vanishing coupling and σ_8 can in principle be broken by observational measurements of the cluster mass function over a sufficiently large mass and redshift range.

4.3 Halo Concentration

As shown in the previous section, deviations of the SO HMF for cDE models from the Λ CDM one increase at higher overdensity. This result suggests that this difference in the HMF is due to a change in the timing of halo collapse induced by the presence of coupling which, in turn, induces a change of the halo density profiles.

Halos in dissipationless N-body simulations of a Λ CDM model have spherically averaged density profiles that are well described by the profiles of Navarro et al. (1997), hereafter NFW. For an NFW halo of a given mass, the halo density profile can be specified entirely by one parameter, the concentration, although the relation between concentration and mass is characterized by a significant intrinsic scatter (e.g. Macciò et al. 2008; Gao et al. 2008; Duffy et al. 2008; Zhao et al. 2009; Prada et al. 2011).

In the following, we use a simple method (see Eqs. 6-9 in Springel et al. 2008) to compute concentrations for the halos identified in our L-CoDECS simulations. According to this method, the characteristic NFW overdensity δ_c is a function of halo concentration c , and can be expressed in terms of the maximum circular velocity of the halo, V_{max} , and the radius r_{max} at which this velocity is attained:

$$\delta_c = \frac{200}{3} \frac{c^3}{\ln(1+c) - c/(1+c)} = 14.426 \left(\frac{V_{max}}{H_0 r_{max}} \right)^2, \quad (22)$$

In Fig. 9, we show the mean concentration c calculated from Eq. (22), as a function of the FoF halo mass. All the cDE models appear to be consistent with the Λ CDM results, with the only exception being represented by the SUGRA003 model. For this model the average concentration is a factor of ~ 2 larger than in Λ CDM at $z = 0$, while gradually approaching the Λ CDM relation at high redshift. This enhanced halo concentration in the SUGRA003 model could provide a way to account for the apparent over-concentration of massive clusters recently found from lensing analyses (e.g. Oguri et al. 2009; Umetsu et al. 2011). On the other hand, if such a high concentration would hold also for typical CDM halos of luminous spiral galaxies (a few $\times 10^{12} h^{-1} M_\odot$), which are not resolved by the simulations analysed here, this specific realization of the ‘‘Bouncing cDE’’ scenario could run into strong tension with the observed dynamical properties of spiral galaxies, as recently investigated by Baldi & Salucci (2011). The enhancement of halo concentration at low redshifts for the ‘‘Bouncing cDE’’ scenario also explains why the HMF of this model shows deviations from Λ CDM only at high overdensity thresholds, $\Delta_c = 500, 1500$, while the FoF HMF and the low overdensity SO HMF (i.e. for $\Delta_c = 200$) is much closer to the expectation from the fiducial Λ CDM model.

5 DISCUSSION AND CONCLUSION

We have investigated in large detail how the halo mass function is affected by different possible types of interaction between dark energy and dark matter. By means of the L-CoDECS suite of large N-body simulations (Baldi 2011b) we have computed the abundance of halos as a function of redshift and mass in six different cosmological models (see Table 1): the fiducial standard Λ CDM scenario, three models of interacting DE with an exponential self-interaction potential and a constant coupling function (EXP001-003), one model with an exponentially growing coupling strength (EXP008e3), and one specific realization of the Bouncing cDE scenario based on a SUGRA self-interaction potential (SUGRA003). In doing so, we have assumed as a single reference scenario the standard concordance Λ CDM cosmology with cosmological parameters consistent with the latest WMAP7 results, and we have constructed all the other cDE models such that they have the same WMAP7 parameters at $z = 0$. This strategy allows us to perform a self-consistent comparison of the footprints of cDE models with respect to the standard Λ CDM cosmology. On the other hand, in order to distinguish the peculiar signatures of a DE-CDM interaction on the growth of structures, from the effects of any other minimally coupled dynamical DE model (such as a *Quintessence* or a *phantom* scalar field) one would need to compare any given cDE scenario to a corresponding dynamical DE cosmology tuned to have the same expansion history. For each of our scenarios, we have then derived both the Friends-of-Friends (FoF) halo mass function and a series of SO mass functions for three values of the overdensity threshold Δ_c , namely $\Delta_c = 200, 500, 1500$, at the present time and at $z = 1$ and 2.

Our findings show that the FoF mass function is significantly affected by the interaction and displays large deviations from the expected Λ CDM halo abundance at $z = 0$, due to the faster growth of density perturbations, with the only exception of the Bouncing cDE scenario that shows very little differences from Λ CDM at the present time. This is expected due to the peculiar dynamics of the Bouncing cDE model that provides the same value of σ_8 as Λ CDM at $z = 0$. In this respect, our results fully confirm previous findings. On the other hand, all the remaining cDE models are characterized by larger values of σ_8 as compared to Λ CDM, and our investigation shows that the effect of the interaction on the mass function is in general highly degenerate with σ_8 , such that the nonlinear halo mass function extracted from the simulations can be quite accurately reproduced by the standard fitting functions computed for the actual value of σ_8 attained by each model. Such degeneracy is however broken by the different redshift evolution of the halo mass function, especially at large masses, in the various cDE models as compared to Λ CDM, such that the same value of σ_8 does not accurately reproduce the abundance of massive halos at different epochs. This is true also for the Bouncing cDE model, which for low overdensity thresholds appears practically indistinguishable from Λ CDM at $z = 0$, but shows a significant excess in the expected number of massive halos at higher redshifts. On the other hand, at higher overdensity thresholds the Bouncing cDE model can be easily distinguished from Λ CDM even at $z = 0$, as the degeneracy with σ_8 is broken and the halo mass func-

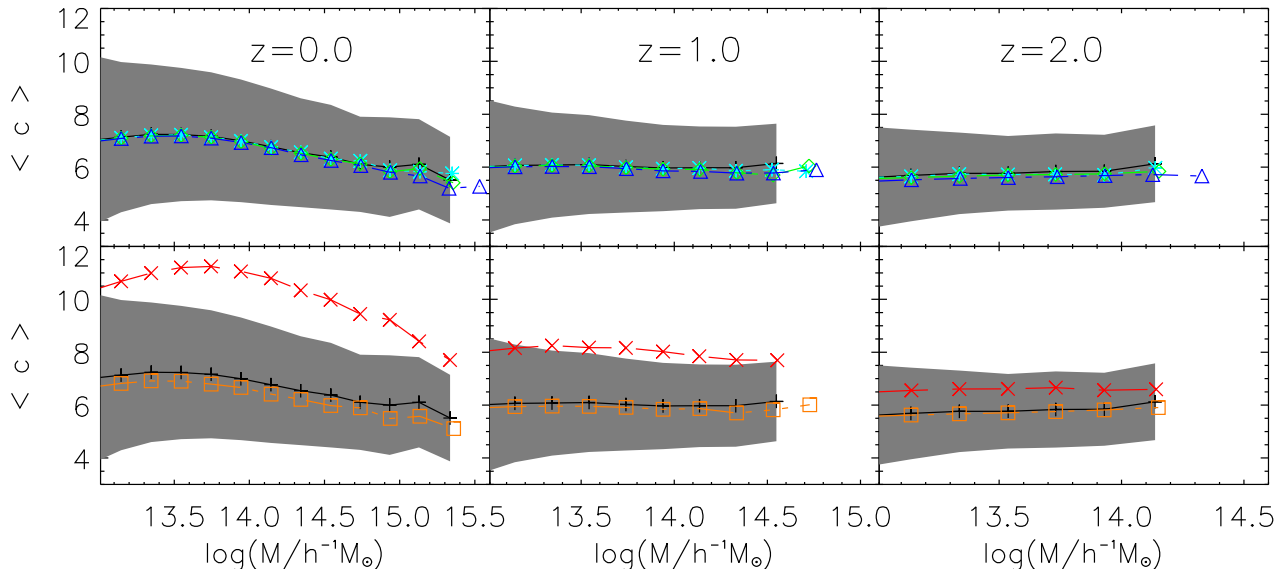


Figure 9. The mean halo concentration as a function of FoF halo mass. The different colors, symbols and line-styles are the same as in the previous figures. The shaded region shows 1σ scatter in the concentration computed within each mass bin. For reasons of clarity it is only shown for the reference Λ CDM simulation.

tion shows a significant enhancement over the expected halo abundance at large masses. We have investigated the origin of this dependence of the deviation from Λ CDM for the Bouncing cDE scenario, and found that the effect is due to a significant increase of the average halo concentration at low redshifts for such cosmology: starting from the same normalization of the concentration-mass relation as Λ CDM at $z = 2$, the Bouncing cDE model produces concentrations that are twice as large as in Λ CDM at $z = 0$.

In a recent analysis Tarrant et al. (2011) computed the linearly-extrapolated critical overdensity for spherical collapse, δ_* , for coupled DE models, with the purpose of including the effect of coupling in the halo mass function. Clearly, including the coupling effect in the computation of δ_* affects the predicted halo abundance when using the expressions by Press & Schechter (1974) (PS) or by Sheth & Tormen (1999) (ST). On the other hand, the fitting functions by Jenkins et al. (2001) (J01) and Tinker et al. (2008) (T08) are not affected by δ_* since their universality makes them to be only functions of the r.m.s. fluctuation amplitude computed at the halo mass scale. While it is beyond the scope of this paper to test the predictions of PS and ST mass functions by accounting for DE coupling on spherical collapse, our results clearly demonstrate that the universal fitting functions by J01 and T08 can not be used to predict mass and redshift dependence of halo counts with an accuracy of 10 per cent or better. This is even more true when dealing with non-standard cDE models, such as the EXP008e3 and SUGRA003 ones.

To conclude, we have investigated the effects of interacting Dark Energy models on the abundance of massive halos as a function of redshift and mass, using different methods to identify halos and to compute their mass. Our results show that a clear degeneracy exists between the coupling and the standard parameter σ_8 , but that both the redshift

evolution and the detailed shape of the high-mass tail of the halo mass function allow to break such degeneracy at some level. Furthermore, we have shown that halo concentrations are very mildly affected by the Dark Energy interactions when the amplitude of density perturbations is normalized at high redshifts (contrarily to what is found for a normalization at $z = 0$) with the only exception of the “Bouncing” coupled Dark Energy scenario that shows a very rapid increase of halo concentrations with respect to the fiducial Λ CDM model at recent epochs. Our study therefore provides a direct way to test interacting Dark Energy models with present and future data on the abundance of massive clusters as a function of redshift. A full exploitation of future cluster surveys to constrain coupled DE models will however require accurately calibrating corrections to expressions of the halo mass function, whose universality has been tested with simulations only within the Λ CDM framework. Clearly, the observational measurement of the evolution of the cluster mass function alone could not provide in itself an incontrovertible test for the presence of cDE. This test should be complemented by other observational probes of large-scale structures. In this framework, the calibration of the HMF for cDE models presented here add an important piece of information that, in combination with other observational constraints, will enable to test and, possibly, to falsify the cDE scenario.

ACKNOWLEDGEMENTS

The authors would like to thank Federico Marulli for valuable discussions. Weiguang Cui acknowledges a fellowship from the European Commission’s Framework Programme 7, through the Marie Curie Initial Training Network CosmoComp (PITN-GA-2009-238356). MB is supported by the DFG Cluster of Excellence “Origin and Structure of the

Universe” and by the TRR33 Transregio Collaborative Research Network on the “Dark Universe”. SB acknowledges partial financial support from the PRIN-INAF-2009 Grant “Towards an Italian Network for Computational Cosmology”, by the PRIN-MIUR-2009 Grant “Tracing the growth of structures in the Universe” and by the PD51-INFN Grant.

REFERENCES

- Allen S. W., Evrard A. E., Mantz A. B., 2011, *ARA&A*, 49, 409
- Amendola L., 2000, *Phys. Rev.*, D62, 043511
- Amendola L., 2004, *Phys. Rev.*, D69, 103524
- Amendola L., Baldi M., Wetterich C., 2008, *Phys. Rev.*, D78, 023015
- Armendariz-Picon C., Mukhanov V. F., Steinhardt P. J., 2001, *Phys. Rev.*, D63, 103510
- Baldi M., 2011a, *MNRAS*, 414, 116
- Baldi M., 2011b, *MNRAS* in press [arXiv:1107.5049]
- Baldi M., 2011c, *MNRAS* Submitted [arXiv:1109.5695]
- Baldi M., 2011d, *MNRAS*, 411, 1077
- Baldi M., Pettorino V., Robbers G., Springel V., 2010, *MNRAS*, 403, 1684
- Baldi M., Salucci P., 2011, *JCAP* in press, arXiv:1111.3953
- Baugh C. M., Gaztanaga E., Efstathiou G., 1995, *Mon. Not. Roy. Astron. Soc.*, 274, 1049
- Beynon E., Baldi M., Bacon D. J., Koyama K., Sabiu C., 2011, arXiv:1111.6974
- Bhattacharya S., Heitmann K., White M., Lukić Z., Wagner C., Habib S., 2011, *ApJ*, 732, 122
- Bode P., Ostriker J. P., Turok N., 2001, *Astrophys. J.*, 556, 93
- Boylan-Kolchin M., Bullock J. S., Kaplinghat M., 2011, arXiv:1111.2048
- Brax P., Martin J., 1999, *Phys. Lett.*, B468, 40
- Clemson T., Koyama K., Zhao G.-B., Maartens R., Valiviita J., 2011, arXiv:1109.6234, * Temporary entry *
- Cohn J. D., White M., 2008, *MNRAS*, 385, 2025
- Courtin J., et al., 2011, *Mon. Not. Roy. Astron. Soc.*, 410, 1911
- Creminelli P., D’Amico G., Norena J., Senatore L., Vernizzi F., 2010, *JCAP*, 1003, 027
- Crocce M., Fosalba P., Castander F. J., Gaztañaga E., 2010, *MNRAS*, 403, 1353
- Cui W., Borgani S., Dolag K., Murante G., Tornatore L., 2011, ArXiv e-prints
- Davis M., Efstathiou G., Frenk C. S., White S. D. M., 1985, *ApJ*, 292, 371
- Dolag K., Borgani S., Murante G., Springel V., 2009, *MNRAS*, 399, 497
- Duffy A. R., Schaye J., Kay S. T., Dalla Vecchia C., 2008, *MNRAS*, 390, L64
- Farrar G. R., Rosen R. A., 2007, *Physical Review Letters*, 98, 17, 171302
- Ferreira P. G., Joyce M., 1998, *Phys. Rev.*, D58, 023503
- Gao L., Navarro J. F., Cole S., et al., 2008, *MNRAS*, 387, 536
- Honorez L. L., Reid B. A., Mena O., Verde L., Jimenez R., 2010, *JCAP*, 1009, 029
- Hu W., Sawicki I., 2007, *Phys. Rev.*, D76, 064004
- Jenkins A., Frenk C. S., White S. D. M., et al., 2001, *MNRAS*, 321, 372
- Komatsu E., et al., 2011, *Astrophys. J. Suppl.*, 192, 18
- Koyama K., Maartens R., Song Y.-S., 2009, *JCAP*, 0910, 017
- Lacey C., Cole S., 1994, *MNRAS*, 271, 676
- Laureijs R., Amiaux J., Arduini S., et al., 2011, ArXiv e-prints
- Lee J., Baldi M., 2011, *ApJ* in press, arXiv:1110.0015
- Lee J., Komatsu E., 2010, *Astrophys. J.*, 718, 60
- Lewis A., Challinor A., Lasenby A., 2000, *Astrophys. J.*, 538, 473
- Lovell M., Eke V., Frenk C., et al., 2011, ArXiv e-prints
- Lucchin F., Matarrese S., 1985, *Phys. Lett.*, B164, 282
- Lukić Z., Heitmann K., Habib S., Bashinsky S., Ricker P. M., 2007, *ApJ*, 671, 1160
- Macciò A. V., Dutton A. A., van den Bosch F. C., 2008, *MNRAS*, 391, 1940
- Marulli F., Baldi M., Moscardini L., 2011, *MNRAS* in press, arXiv:1110.3045
- More S., Kravtsov A., Dalal N., Gottlöber S., 2011, ArXiv e-prints
- Navarro J. F., Frenk C. S., White S. D. M., 1997, *ApJ*, 490, 493
- Oguri M., Hennawi J. F., Gladders M. D., et al., 2009, *ApJ*, 699, 1038
- Perlmutter S., et al., 1999, *Astrophys. J.*, 517, 565
- Pettorino V., Baccigalupi C., 2008, *Phys. Rev.*, D77, 103003
- Prada F., Klypin A. A., Cuesta A. J., Betancort-Rijo J. E., Primack J., 2011, ArXiv e-prints
- Press W. H., Schechter P., 1974, *ApJ*, 187, 425
- Ratra B., Peebles P. J. E., 1988, *Phys. Rev.*, D37, 3406
- Reed D., Gardner J., Quinn T., et al., 2003, *MNRAS*, 346, 565
- Reed D. S., Bower R., Frenk C. S., Jenkins A., Theuns T., 2007, *MNRAS*, 374, 2
- Riess A. G., et al., 1998, *Astron. J.*, 116, 1009
- Rudd D. H., Zentner A. R., Kravtsov A. V., 2008, *ApJ*, 672, 19
- Schmidt B. P., et al., 1998, *Astrophys. J.*, 507, 46
- Sheth R. K., Tormen G., 1999, *MNRAS*, 308, 119
- Springel V., 2005, *Mon. Not. Roy. Astron. Soc.*, 364, 1105
- Springel V., Wang J., Vogelsberger M., et al., 2008, *MNRAS*, 391, 1685
- Springel V., White S. D. M., Tormen G., Kauffmann G., 2001, *MNRAS*, 328, 726
- Stanek R., Rudd D., Evrard A. E., 2009, *MNRAS*, 394, L11
- Tarrant E. R. M., van de Bruck C., Copeland E. J., Green A. M., 2011, ArXiv e-prints
- Tarrant E. R. M., van de Bruck C., Copeland E. J., Green A. M., 2011, arXiv: 1103.0694
- Thomas S. A., Abdalla F. B., Lahav O., 2011, *Phys.Rev.Lett.*, 106, 241301
- Tinker J., Kravtsov A. V., Klypin A., et al., 2008, *ApJ*, 688, 709
- Umetsu K., Broadhurst T., Zitrin A., Medezinski E., Hsu L.-Y., 2011, *ApJ*, 729, 127
- Warren M. S., Abazajian K., Holz D. E., Teodoro L., 2006, *ApJ*, 646, 881
- Weinberg S., 1989, *Rev. Mod. Phys.*, 61, 1

- Wetterich C., 1988, Nucl. Phys., B302, 668
Wetterich C., 1995, Astron. Astrophys., 301, 321
White M., 2001, A&A, 367, 27
White M., 2002, ApJS, 143, 241
White S. D. M., 1994, arXiv: astro-ph/9410043
Zel'dovich Y. B., 1970, Astron. Astrophys., 5, 84
Zhao D. H., Jing Y. P., Mo H. J., Börner G., 2009, ApJ,
707, 354